JOURNAL OF MATERIALS SCIENCE 16 (1981) 3357–3364

Characterization of crystallization in Metglas 2826 MB alloy*

K. P. MIZGALSKI, O. T. INAL
Department of Metallurgical and Materials Engineering, New Mexico Institute of Mining and Technology, Socorro, New Mexico 87801, USA

F. G. YOST, M. M. KARNOWSKY
Sandia Laboratories, Albuquerque, New Mexico 87185, USA

The crystallization behaviour of the Metglas 2826 MB alloy* ($Fe_{40}Ni_{38}Mo_4B_{18}$) has been studied using resistance measurements and X-ray diffraction techniques. Three annealing sequences were used to follow the process. Samples were annealed isothermally (a) at 780° C in a vacuum of 2×10^{-5} torr for times in the range 1 sec to 4 h, (b) for 2 h in an argon atmosphere at temperatures where the resistance curve indicated phase changes to occur, and (c) for 300 h in 100 torr of helium at 400, 600, 700 and 850° C. From these annealing sequences it was found that the alloy did not crystallize below 410° C and followed a crystallization process of: amorphous $Fe_{40}Ni_{38}Mo_4B_{18} \rightarrow Fe_xNi_{23-x}B_6$ (cubic) + glassy matrix $\rightarrow Fe_xNi_{23-x}B_6$ + (Fe, Ni) (FCC) $\rightarrow$ $(Fe, Ni)_3B$(bct). This series of transformations was followed for Sequences (a) and (c) above, but was slightly different for Sequence (b). An orthorhombic $(Fe, Ni)_3B$ phase was found in the samples annealed in a vacuum of 2×10^{-5} torr.

1. Introduction

Metglas 2826 MB alloy* with composition $Fe_{40}Ni_{38}Mo_4B_{18}$ is a ferromagnetic, high permeability nickel–iron metallic glass which, when appropriately annealed, yields magnetic properties similar to those of higher nickel permalloys. In the as-cast condition, this material has a useful balance of magnetic and mechanical properties which makes it suitable for use in flexible magnetic shielding applications. Field annealing at 355° C develops optimum magnetic properties, but with some loss in mechanical properties. Field annealing raises the hardness and wear resistance of the material so it is attractive for magnetic tape head uses. This magnetic alloy is also suitable for applications in magnetic core devices such as transformers and motors with small core losses [1].

Interest in the annealing behaviour of amorphous alloys has developed from the need to understand the thermal stability of these alloys for potential commercial applications. The nature of the crystallization nuclei and the mechanism of growth in an undercooled liquid leads to the possibility of producing useful microstructures (by total or partial crystallization of an amorphous alloy) unobtainable by other means [2].

The purpose of this study was to investigate the crystallization behaviour and the associated changes in the properties of the Metglas 2826 alloy ($Fe_{40}Ni_{38}Mo_4B_{18}$). Annealing of the alloy was carried out isothermally at 780° C, and at various temperatures for periods of 300 h. The crystallization process was followed by analyses of resultant structures and properties using X-ray diffraction and resistance against temperature or time curves.

2. Experimental procedure

All of the procedures in this study were carried out using samples cut from a ribbon (25.4 mm

*Trademark of Allied Chemical Co.

0022–2461/81/123357–08$02.80/0 © *1981 Chapman and Hall Ltd.*

wide x 0.051 mm thick) of Metglas 2826 MB alloy with the composition $Fe_{40}Ni_{38}Mo_4B_{18}$.

2.1. Resistance curves

The technique of monitoring changes in electrical resistance was used to determine temperature regimes where significant microstructural alterations occurred. Resistance measurements were made using a four-pole reversing polarity apparatus using a constant current of 0.1 A flowing through the sample. The resistance measurements were normalized to give the per cent change in resistance which eliminates dimensional effects. A more detailed discussion of this procedure is given elsewhere [3]. The samples were encapsulated in quartz tubes under vacuum and annealed. Measurements were made on the alloy while being heated over the temperature range from room temperature to 800° C. Inflection points in the curve thus obtained were taken as an indication of microstructural changes occurring in the sample.

In addition to the temperature survey, samples were heated isothermally at 425° C (just above the crystallization temperature of 410° C [4]) and 700° C. From the resistance measurements, taken at these temperatures for different times during the annealing, curves of per cent change in resistance against time were constructed to determine the length of time needed to reach equilibrium structure at each of these temperatures.

A plot of per cent change in resistance against temperature is shown in Fig. 1 for the temperature survey from room temperature to 800° C. Inflection points, Points A, B, C, D and E, are seen to occur at temperatures of 410, 490, 540, 660 and 790° C, respectively. Fig. 2 shows a plot of per cent change in resistance against time for the alloy heated isothermally at 425° C. The curve shows that only one phase change occurs (Point A) during the heat treatment period shown on the graph. Fig. 3 shows a plot of per cent change in resistance against annealing time for the alloy treated isothermally at 700° C. The curve shows that the alloy goes through several more phase changes (Points A, B, C and D) and the equilibrium structure is not reached at this temperature until after approximately 20 h. The letters superimposed on the graphs in Figs 1 to 3 attempt to indicate

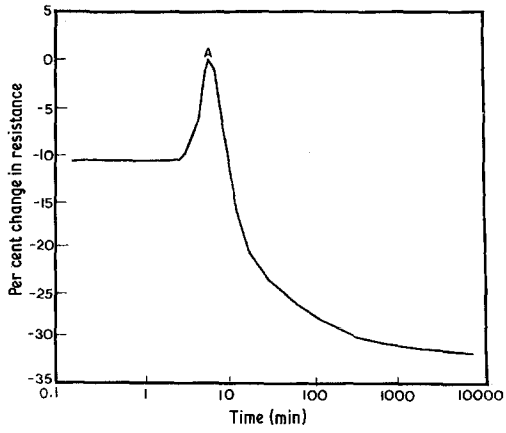

Figure 2 Graph of per cent change in resistance against time for the alloy heated at 425° C.

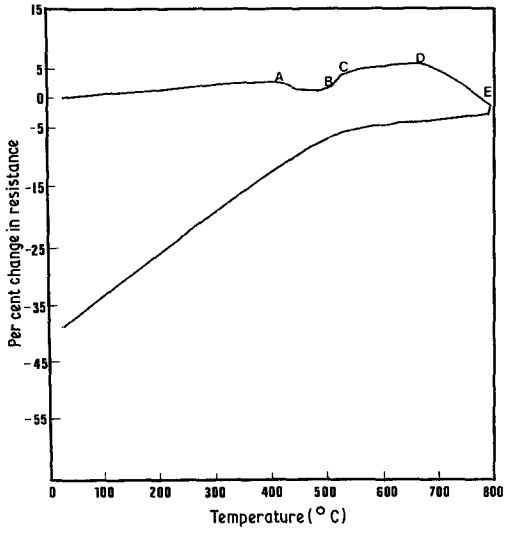

Figure 1 Temperature survey for 2826 MB alloy as a graph of per cent change in resistance against temperature.

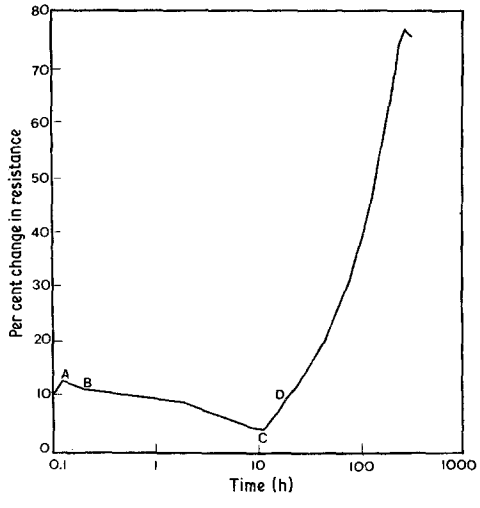

Figure 3 Graph of per cent change in resistance against time for the alloy heated at 700° C.

the phase changes that occur in the alloy under the different heating conditions utilized.

2.2. X-ray diffraction analyses

A Philips X-ray diffractometer equipped with a single crystal monocromator was used to analyse the amorphous, as well as the heat-treated, samples (operated at 40 kV and 20 mA using FeKα radiation).

Using the results of the temperature survey, samples were annealed at temperatures where a phase is indicated by the curve. Samples were heated, therefore, at 420, 500, 550, 670 and 800° C. Utilizing these samples and the samples heated isothermally at 780° C and the samples heated for 300 h at 400, 425, 600 700 and 850° C, phase analyses were performed using X-ray diffraction techniques. Four different phases were encountered in the samples, depending on the heat treatment. These different phases were a face-centered cubic (Fe, Ni) solid solution, a cubic $Fe_xNi_{23-x}B_6$ phase, a tetragonal $(Fe, Ni)_3B$ phase and an orthorhombic $(Fe, Ni)_3B$ phase. Table I shows the diffraction data for the (Fe, Ni) solid solution. This phase had a lattice constant of 0.358 nm which, if Vegrad's Rule is followed, has the composition of approximately 51% Fe and 49% Ni. The intensities of the diffraction peaks were calculated using the standard face-centered cubic atom positions.

Table II shows the diffraction data for the cubic boride phase $Fe_xNi_{23-x}B_6$ which has a lattice constant of 1.0547 nm. The space group of this unit cell is $Fm3m$ and the intensities were calculated using the atomic positions given for $Cr_{23}C_6$ in [5] since $Cr_{23}C_6$ is isostructural with the cubic boride phase and their unit cells are approximately the same size.

Table III shows the diffraction data for the tetragonal $(Fe, Ni)_3B$ phase which has lattice constants of $a_0 = 0.8918$ and $c_0 = 0.4404$ nm. The space group of this unit cell is $P4_2/n$ and the intensities were calculated using the atomic positions given by Rundquist [6] for a phase with the composition $Fe_3P_{0.37}B_{0.63}$.

Table IV is the diffraction data for the orthorhombic $(Fe, Ni)_3B$ phase with the lattice constants $a_0 = 0.4436$, $b_0 = 0.5354$ and $c_0 = 0.6614$ nm. All reflections were consistent with the space group $Pnma$ and the intensities were calculated using the atomic parameters given by Rundquist [7] for the phase Ni_3B.

TABLE I Diffraction data for (Fe, Ni) solid solution (fcc): $a_0 = 0.3586$ nm

hkl	d_{obs}* (nm)	d_{calc} (nm)	I_{obs}†	I_{calc}‡
111	0.2064	0.2070	100	29.7
200	0.1787	0.1793	45	13.5
220	0.1266	0.1268	35	16.0
311	0.1081	0.1081	35	24.0

* The values of d_{obs} were calculated with Fe.
† $I_{obs} = I/Id = 0.2064$ (nm).
‡ $I_{calc} = p|F|^2$ (L.P.F.) $\times 10^{-4}$.

To aid in the determination of the phases present in the samples a least-squares unit-cell refinement procedure developed by Evans *et al.* [8] was used to determine the calculated d-spacing and the lattice constants of the unit cells. When calculating the intensities of the diffraction peaks, equations for the structure factors of each unit cell were obtained from [9]. For each of the boride phases it was assumed that the amount of iron and nickel in the compound was in the same ratio as the solid solution and thus a weighted average was used for the atomic scattering factor in the structure factor calculations.

2.3. Phase transformations

Table V gives a summary of the transformations occuring in the alloy when it is heated in the temperature range from room temperature to 800° C for 2 h in an argon atmosphere. The alloy remains non-crystalline up to 410° C, but once this temperature is reached, the cubic boride phase starts to precipitate out of the amorphous matrix. At this temperature some of the alloy is still in the amorphous state, as is evident by the broad, diffuse diffraction peaks of the cubic boride phase. After heating at 500° C for 2 h, the remaining amorphous matrix crystallizes and the alloy then contains a mixture of the cubic boride and the (Fe, Ni) solid solution. At 550° C, the phases are the same but the amount of (Fe, Ni) solid solution is seen to increase at the expense of the cubic boride phase. When heated to 670° C, the tetragonal boride appears in the alloy, again, at the expense of the cubic boride phase. Finally, at 800° C, only the tetragonal boride and (Fe, Ni) solid solution phases are present. The percentage of each phase was calculated using the direct comparison method outlined by Cullity [10]. These percentages indicate that the amount of boride phase in the alloy decreases as the annealing temperature is increased.

The alloy heated for 300 h at 400° C exhibits

TABLE II Diffraction data for $Fe_xNi_{23-x}B_6$ (Cubic): $a_0 = 1.0547$ nm

hkl	d_{obs} (nm)	d_{calc} (nm)	I_{obs}*	I_{calc}†
311	0.318	0.318	10	3.52
222	0.302	0.304	10	4.0
400	0.264	0.264	10	33
420	0.2362	0.2358	30	114
422	0.2157	0.2153	40	120
333, 511	0.2033	0.2030	100	428
440	0.1870	0.1865	30	77.2
531	0.1776	0.1783	Overlap with (Fe, Ni)	107
600, 442	0.1752	0.1758	20	70.9
533	0.1604	0.1808	10	18.2
622	0.1586	0.1590	20	27.2
800	0.1318	0.1318	15	12.1
820, 644	0.1279	0.1279	20	40.2
822, 660	0.1274	0.1243	35	116
751, 555	0.1218	0.1218	24	74.3
840	0.1180	0.1179	15	28.8
753, 911	0.1159	0.1158	20	50.5
931	0.1106	0.1106	15	25.7

* $I_{obs} = I/Id = 0.2033$ (nm)
† $I_{calc} = p|F|^2$ (L.P.F) $\times 10^{-10}$

no crystallization and the diffraction pattern shows only short-range order. Table VI gives a summary of the equilibrium phases and their volume fractions evaluated in each case. After heating at 600° C for 300 h the equilibrium phases are the cubic boride phase and the (Fe, Ni) solid solution. At 700° C, some of the cubic boride is seen to be transformed to the tetragonal boride phase and, at 850° C only the tetragonal boride remains together with the (Fe, Ni) solid solution. It is interesting to note that during this annealing sequence the amount of (Fe, Ni) solid solution remains fairly constant and only the amounts of the boride phases appear to change.

TABLE III Diffraction data* for $(Fe, Ni)_3B$ (tetragonal): $a_0 = 0.8918$ nm and $c_0 = 0.4404$ nm

hkl	d_{obs} (nm)	d_{calc} (nm)	I_{calc}†
201	0.314	0.313	50.6
211	0.296	0.295	6.0
310	0.284	0.283	30.0
221	0.2563	0.2565	8.5
301	0.2458	0.2464	30.6
102	0.2129	0.2137	18.8
112	‡	0.2079	144
401	0.1986	0.1989	15.1
421	0.1811	0.1816	5.4
511	0.1626	0.1628	2.0
440	0.1573	0.1576	10.4
203	0.1396	0.1394	11.4
621	0.1344	0.1343	14.6
631	0.1276	0.1273	28.3
641	0.1191	0.1190	3.1
622	0.1187	–	–

* Due to overlap of the strongest reflection with the (111) (Fe, Ni) reflection, I_{obs} is not given.
† $I_{calc} = p|F|^2$ (L.P.F.) $\times 10^{-6}$
‡ Overlap with (111) (Fe, Ni) reflection.

For the third annealing sequence, samples were heated at 780° C in vacuum for varying lengths of time. Table VII gives a summary of the X-ray data obtained from this annealing sequence. In the amorphous state, the diffraction pattern indicated the presence of random atomic distribution in the alloy, but after heating for approximately 1 sec at 780° C short-range order was seen to be induced in the sample. After 5 sec of annealing diffraction peaks are seen to appear for the cubic boride phase and the (Fe, Ni) solid solution with the cubic boride being the predominant phase. After 10 sec, diffraction peaks appear for the orthorhombic $(Fe, Ni)_3B$ phase which was not seen in either of the other two annealing sequences. The sample is not fully crystalline until after 30 sec, as evidenced by the increasing intensities of the diffraction peaks. Also after 30 sec, diffraction lines appear indicating the presence of the tetragonal boride phase. After annealing for from 45 sec to 15 min all four of the phases are seen to be present with the cubic boride and the (Fe, Ni) solid solution being the predominant phases. After 4 h the phases present in the alloy are the (Fe, Ni) solid solution, the orthohombic boride, and the tetragonal boride phases.

TABLE IV Diffraction data for $(Fe, Ni)_3B$(ortho): $a_0 = 0.4436$ nm, $b_0 = 0.5354$ nm and $c_0 = 0.6614$ nm

hkl	d_{obs} (nm)	d_{calc} (nm)	I_{obs}*	I_{calc}†
112	0.2371	0.2376	70	14.1
121	0.2161	0.2166	65	185
201	0.2109	0.2103	50	359
022	0.2079	0.2081	100	334
210	0.2043	0.2049	85	286
103	0.1974	0.1974	100	241
211	0.1954	0.1957	75	54.5
122	0.1882	0.1884	65	176
113	0.1851	0.1852	60	207
212	0.1734	0.1741	50	26.9
220	0.1704	0.1708	35	9.1
211	0.1655	0.1654	55	84.3
004	–	0.1653	–	–
203	0.1567	0.1563	30	2.0
114	–	0.1488	30	94.2
132	–	0.1481	–	–
311	0.1390	0.1393	30	45.8
230	–	0.1390	–	–
033	–	0.1387	–	–
124	0.1340	0.1341	30	30.2
040	–	0.1339	–	–
(312)	0.1309	0.1308	40	3.0
(232)	0.1282	0.1282	40	179
042	0.1243	0.1241	35	18.1
313	0.1198	0.1197	40	28.7
224	0.1188	0.1188	35	3.8
233	0.1175	0.1176	55	13.1
134	–	0.1170	–	–

* $I_{obs} = I/Id = 0.2079$ nm.
† $I_{calc} = p|F|^2$ (L.P.F.) $\times 10^{-5}$

3. Discussion

3.1. Phase analyses

The phase analyses may be somewhat inaccurate for a number of reasons.

It should be noted that the molybdenum atoms in the alloy, when heated, are assumed to substitutionally replace iron and nickel atoms. For example, in fact, the (Fe, Ni) solid solution is actually an (Fe, Ni, Mo) solid solution, and the same holds true for the other phases present in the samples. Since the percentage of molybdenum in the alloy is small, it was ignored in calculating the atomic scattering factor used in determining the structure factors of the phases.

Another source of error in the intensity calculations may come from the atomic parameters used in calculating the structure factors of the different boride phases. Because the atomic parameters used in the calculations were for compounds that were only close in composition to the phases observed, as in the case of the tetragonal and orthorhombic borides, or completely different, as in the case of the cubic boride, there should be an effect on the intensity calculations. However, because the atomic positions used in the calculations were from compounds that were isostructural and had approximately the same lattice constants as the phases actually observed, these parameters were used in the calculations.

Also, the values of the observed peak intensities are high in some instances due to overlapping diffraction peaks. Because the height of the peak was used and not its area, this could also have an effect on the values given for the observed intensities.

There might also be a discrepancy between the observed intensity, I_{obs}, and the calculated intensity I_{calc}, at higher diffraction angles because the temperature factor was neglected in the equation used to compute the intensity values.

If all these assumptuous and errors are considered, it can be seen that the calculated intensities can only be approximate. Since the calculated intensities were used to determine the volume percentages given in Tables V and VI, these percentages are also subject to the errors outlined above.

3.2. Phase transformations

When Metglas 2926 MB alloy is annealed, the first phase to appear is the cubic boride phase. The fact that a boride phase is the first to crystallize in an iron–nickel base metallic glass is in agreement with work already published [11–13]. The existence of a cubic boride has only been reported by Franke *et al.* [14], and it was found in a splat-cooled $Fe_{95}B_5$ alloy. The crystal structure of this phase was also ascribed to a $Cr_{23}C_6$ structure and the equivalent Fe–B phase was thought to be

TABLE V Phase transformations of 40Fe–38Ni–4Mo–18B upon annealing in an argon atmosphere for 2 h

Annealing temperature (°C)	Transformation
420	Amorphous → $Fe_xNi_{23-x}B_6$ + Amorphous
500	$Fe_xNi_{23-x}B_6$ (45%) (fcc) + (Fe, Ni) (55%) (fcc)
550	$FeNi_{23-x}B_6$ (36%) (fcc) + (Fe, Ni) (64%) (fcc)
670	$(Fe, Ni)_3B$ (11%) (tet) + $Fe_xNi_{23-x}B_6$ (14%) (fcc) + (Fe, Ni) (75%) (fcc)
800	$(Fe, Ni)_3B$ (10%) (tet) + (Fe, Ni) (90%) (fcc)

TABLE VI Equilibrium phases of initially amorphous 40Fe–38Ni–4Mo–18B annealed for 300 h in vacuum

Annealing temperature (°C)	Phases present
400	Only short-range order present
600	78% (Fe, Ni) + 22% $Fe_xNi_{23-x}B_6$ (cub)
700	68% (Fe, Ni) + 14% $Fe_xNi_{23-x}B_6$ + 18% $(Fe, Ni)_3B$ (tet)
850	73% (Fe, Ni) + 27% $(Fe, Ni)_3B$ (tet)

$Fe_{23}B_6$. Until the present work, there has been no report on the existence of this cubic boride crystallizing in a metallic glass with a metalloid content in the range of 15 to 20 at %. This could possibly be attributed to the presence of the molybdenum in the 2826 MB alloy, although there is no apparent effect of Ni on the crystallization behaviour of $Fe_{50}Ni_{30}B_{20}$ alloy compared with the $Fe_{80}B_{20}$ alloy [15].

The metalloid determines the shape and structure of the crystals formed by the crystallization of amorphous alloys. For example, Metglas 2826 A alloy* ($Fe_{32}Ni_{36}Cr_{14}P_{12}B_6$) first exhibits precipitates of (Fe, Ni) solid solution in the amorphous matrix instead of a boride phase [14]. The (Fe, Ni) precipitates contain no P and the quantity of Cr is reduced compared with the glassy matrix. The glassy matrix then crystallizes to a $(Ni, Cr, Fe)_3(P, B)$-type tetragonal structure. Other work [16] suggests that, for Fe–B alloys with less than 17 at % B, the first crystalline phase to precipitate on isothermal annealing is α-Fe. The 2826 MB alloy has a slightly higher B-content and it is believed that this is the reason for the cubic boride phase to crystallize in the annealing sequences outlined in Tables V and VII. At 410° C the cubic boride phase begins to nucleate and grow. The glassy matrix apparently becomes depleted in B and, when the temperature gets high enough, (490° C in this case) the glass matrix crystallizes to the (Fe, Ni) solid solution. The cubic boride and (Fe, Ni) solid solution phases appear to crystallize simultaneously during the isothermal anneal at 780° C but this is possibly due to the high annealing temperature used. This is in contrast to the 2826 A alloy where the initial crystallization is controlled by nucleation and the accompanying P and Cr diffusion away from the (Fe, Ni) solid solution and glassy matrix interface [14].

Other studies cited here indicate that there is a definite correlation between the crystallization behaviour of a particular amorphous alloy and the

TABLE VII Phase transformations for Metglas 2826 MB alloy annealed under vacuum at 780° C

Annealing time	Summary of X-ray data
Amorphous	Random
1 sec	Short-range order (small grains)
5 sec	$Fe_xNi_{23-x}B_6$, cubic (a_0 = 1.0547 nm) Predominant (Fe, Ni) fcc (a_0 = 0.3586 nm), 517. Fe–497. Ni
10 sec	Appearance of $(Fe, Ni)_3B$, orthorhombic (a_0 = 0.4436 nm, b_0 = 0.5354 nm, c_0 = 0.6614 nm)
15 sec	Amount of (Fe, Ni) and $(Fe, Ni)_3B$ increasing at expense of amorphous matrix
30 sec	Proportions of (Fe, Ni) and $Fe_xNi_{23-x}B_6$ phases approximately equal. Appearance of weak lines corresponding to $(Fe, Ni)_3B$, Tetragonal (a_0 = 0.8919 nm, c_0 = 0.4404 nm). Crystallization appears completed.
45 sec–15 min	All of the above phases present, but relative amounts change. (FeNi) and $Fe_xNi_{23-x}B_6$ predominant. Diffraction peaks sharpen.
30–45 min	$Fe_xNi_{23-x}B_6$ phase disappears. Relative amounts of remaining phases increase.
1–1.25 h	$Fe_xNi_{23-x}B_6$ reappears and amount increases at the expence of $(Fe, Ni)_3B$ (ortho) and $(Fe, Ni)_3B$ (tet) phase.
$1\frac{1}{2}$ h	Amount of $Fe_xNi_{23-x}B_6$ decreases again.
$1\frac{3}{4}$ h	$Fe_xNi_{23-x}B_6$ disappears.
2 h	$Fe_xNi_{23-x}B_6$ reappears.
$2\frac{1}{4}$–4 h	$Fe_xNi_{23-x}B_6$ disappears again. Equilibrium phases? (Fe, Ni), $(Fe, Ni)_3B$ (ortho, $(Fe, Ni)_3B$ (tet).

type and amount of metalloid present in the alloy. In the present study, there is also an indication that the type of metal atoms present in the alloy can also affect the crystallization behaviour; for example the presence of the small amout of Mo possibly causing the cubic boride to be the stable low-temperature phase of the 2826 MB alloy.

When the 2826 MB alloy is annealed at higher temperatures, the cubic boride begins to transform to the tetragonal boride structure. This tetragonal phase is the body-centered structure seen in the earlier studies, but not the primative tetragonal structure reported in another study [15]. In other alloys, this bct phase has been observed to be stable at lower temperatures. In the amorphous alloy $Fe_{80}B_{20}$, as the temperature is increased, the $(Fe, Ni)_3B$ (bct) is seen to transform to a $(Fe, Ni)_2B$ (tetragonal) structure. However, the tetragonal boride phase in the present study appears to form a three-phase mixture at 660° C with the cubic boride and the (Fe, Ni) solid solution. Finally, at 790° C, all the cubic boride is seen to be transformed to the tetragonal boride phase leaving a two-phase mixture with the (Fe, Ni) solid solution. The tetragonal boride is seen to be present in the 2826 MB alloy even after annealing at the highest temperature used in this study, 850° C. In this alloy the tetragonal boride phase is seen to be a high-temperature phase rather than a low-temperature phase.

The annealing sequences summarized in Tables V and VI are in agreement, in terms of the phase transformations occurring as the annealing temperature is increased. The only difference seen in Tables V and VI is the amount of boride phase in the samples annealed in argon. The percentage of boride phase in the samples decreases with increased temperature, whereas the percentage of boride phase in the samples annealed in vacuum remains relatively constant. Stubicar *et al.* [12] reported that, for a $Fe_{40}Ni_{40}B_{20}$ glass, the first crystalline phase to appear is an orthorhombic $(Fe, Ni)_3B$ phase, but at higher temperatures, this phase is seen to anneal-out leaving only an (Fe, Ni) solid solution. These authors claim that the boron component diffuses in the amorphous phase to the grain boundaries and/or to the surface of the samples. This phenomenon is seen to occur in samples annealed in vacuum at temperatures greater than 700° C. This was not observed in our study and is in agreement with Liebermann (as indicated by Stubicar *et al.* [11]) who found boride and solid solution phases in the $Fe_{40}Ni_{40}B_{20}$ alloy even when annealed at 1000° C. For the samples annealed in argon it would appear that the boride phase anneals out of the samples, as reported by Stubicar *et al.*, but, in the study reported, this is believed to be for a different reason: impurities in the argon gas possibly reacted with boron as the annealing temperature is increased. A thin oxide coating was evident on the surface of the sample annealed at 800° C, but the diffraction pattern did not show any extra diffraction peaks to aid in identifying this coating.

The series of phase transformations seen in the isothermal annealing at 780° C, summarized in Table VII, is similar to the other two annealing sequences. At this high temperature, the crystallization process starts rapidly with the cubic boride appearing first, followed by the (Fe, Ni) solid solution. This is followed by the crystallization of the orthorhombic boride $(Fe, Ni)_3B$ which was not seen in the other two annealing sequences. Weak diffraction lines from the tetragonal boride eventually appeared after annealing for 30 sec at 780° C, but the diffraction peaks did not reach the intensity of the tetragonal boride phase seen in the other annealing sequences. At longer annealing times, the (Fe, Ni) solid solution became the predominant phase and the cubic boride phase annealed-out, corresponding to the transformations seen in the other annealing sequences. In this case, however, the remaining phases are the (Fe, Ni) solid solution and the orthorhombic and tetragonal boride phases with the orthorhombic phase being the predominant boride. This annealing sequence was carried out in a vacuum of approximately 2×10^{-5} torr, whereas the other two sequences were carried out in argon at atmospheric pressure and in a low vacuum of approximately 100 torr of helium, possibly suggesting that the orthorhombic boride is the stable high-temperature phase in a high vacuum with the tetragonal phase being the stable phase at higher pressures.

5. Conclusions

Resistance measurements performed within the temperature range 25 to 850° C have shown that the 2826 MB alloy goes through a series of transformations upon continuous heating that occur at 410, 490, 540, 660 and 790° C. Crystallization starts at 410° C by the formation of the cubic boride phase $Fe_xNi_{23-x}B_6$. The structural changes observed by X-ray diffraction can be summarized

as: amorphous $Fe_{40}Ni_{38}Mo_4B_{18} \rightarrow Fe_xNi_{23-x}B_6$ + glass matrix $\rightarrow Fe_xNi_{23-x}B_6$ + (Fe, Ni) solid solution $\rightarrow Fe_xNi_{23-x}B_6$ + (Fe, Ni) + $(Fe, Ni)_3B(tet)$ $\rightarrow$ (Fe, Ni) + $(Fe, Ni)_3B(tet)$. The molybdenum in the alloy is assumed here to be in the substantial solid solution.

When the alloy is annealed in a vacuum of 2×10^{-5} torr, the above sequence is changed by the presence of an orthorhombic boride phase, $(Fe, Ni)_3B$. At high temperatures this is the metastable boride phase along with the tetragonal boride phase while in the above sequence the orthorhombic phase does not appear, as indicated.

This study and previously published works indicate that the crystallization process of an amorphous alloy can be affected by the amount and type of metalloid present in the alloy, by the addition of another type of metal atom to an iron–nickel base metallic glass, and by the ambient pressure used in the annealing process.

Acknowledgement

The authors would like to thank Dr L. Keller of UCLA for valuable discussions concerning X-ray diffraction techniques used in this study. Research and Development Division of NMIMT is also acknowledged for partial support of this project.

References

1. Allied Chemical Co. Fact Sheet on Metglas Alloy 2826 MB.
2. M. G. SCOTT, *J. Mater. Sci.* **13** (1978) 291.
3. M. M. KARNOWSKY, *ibid.* **13** (1978) 2339.
4. R. B. ARONSON, *Machine Design* **48** (1976) 20.
5. R. G. WYCKOFF, "Crystal Structures" 2nd edn (Wiley-Interscience, New York, 1964).
6. S. RUNDQUIST, *Acta Chem. Scandinavica* **16** (1962) 1.
7. *Idem, ibid.* **12** (1958) 658.
8. H. T. EVANS, D. E. APPLEMAN and D. S. HANDWERKER; Proceedings of the Meeting of the American Crystallographic Association, Cambridge, Mass, March 1963 (American Crystallographic Association, Cambridge, Mass., 1963) p. 42.
9. F. M. NOSMAN, H. LOUDSDALE and K. LOUDSDALE, "International Tables for X-ray Crystallography" Vol. 1 (The Kynock Press, Birmingham, 1952).
10. B. D. CULLITY, "Elements of X-ray Diffraction" 2nd edn (Addison-Wesley Publishing Co, Reading, Mass, 1978) p. 411.
11. J. L. WALTER, P. RAO, E. F. KOCH and S. F. BARTRAM, *Metal. Trans.* 8A (1977) 1141.
12. M. STUBICAR, E. BABIC, D. SUBASIC, D. PAVUNA and Z. MAROHNIC, *Phys. Stat. Sol. (a)* **44** (1977) 339.
13. J. L. WALTER, S. F. BARTRAM and R. RUSSELL, *Metal. Trans.* 9A (1978) 803.
14. M. VON HEIMENDAHL and G. MAUSSNER, Proceedings of the International Conference on Rapidly Quenched Metals, University of Sussex, Brighton, July, 1978, Vol. 1 (Metals Society, London, 1978) p. 424.
15. O. T. INAL, L. KELLER and F. YOST, *J. Mater. Sci.* **15** (1980) 1947.
16. R. RAY, R. HASEGAWA, C. P. CHOU and L. A. DAVIS, *Scripta Met.* **11** (1977) 973.

Received 11 February and accepted 20 May 1981.